Z. Phys. Chem. **219** (2005) 699–714

SACM/CT Study of Product Energy Distributions in the Dissociation of *n*-Propylbenzene Cations

By J. Troe[1,*], V. G. Ushakov[2], and A. A. Viggiano[3]

[1] Institute for Physical Chemistry, University of Göttingen, Tammannstrasse 6, D-37077 Göttingen, Germany
[2] Institute of Problems of Chemical Physics, Russian Academy of Sciences, 142432 Chernogolovka, Russia
[3] Air Force Research Laboratory, Space Vehicles Directorate, 29 Randolph Rd, Hanscom AFB, MA 01731-3010, USA

Dedicated to Prof. Dr. Jürgen Wolfrum at the occasion of his 65th birthday

(Received January 13, 2005; accepted January 24, 2005)

Reaction Kinetics / Unimolecular Reactions / Ion Fragmentations

The distribution of translational, rotational, and vibrational energies in the fragments (benzylium ions and ethyl radicals) of the dissociation of *n*-propylbenzene cations has been determined by statistical adiabatic channel model/classical trajectory (SACM/CT) calculations. The reaction was treated by CT calculations of capture processes for transitional modes, starting with specified fragment energies. A short-range valence/long-range ion-induced dipole potential model for the transitional modes was employed. The derived distributions approach the results from phase space theory (PST) at small energies and angular momenta. At larger energies and angular momenta, the shapes of the distribution functions remain similar to those from PST; however, the average translational, rotational, and vibrational energies of the fragments increasingly differ from PST predictions. The present results are consistent with separate SACM/CT calculations on the same potential of specific rate constants $k(E, J)$ and thermally averaged rate constants $k_\infty(T)$ of the dissociation/recombination reaction.

1. Introduction

Translational product energy distributions (TPEDs) constitute important observables characterizing the dynamics of unimolecular dissociation processes.

* Corresponding author. E-mail: shoff@gwdg.de

Some information exists for dissociations of neutral molecules, but TPEDs have most frequently been measured for the fragmentation of molecular ions. The available experimental techniques have well been described in the monograph by T. Baer and W. L. Hase [1]. Particularly important techniques that measure TPEDs are PEPICO (photoelectron photoion coincidence) and MIKES (mass analyzed ion kinetic energy spectroscopy). The measured TPEDs have been analysed by a variety of models, which also have been summarized in [1]. The most useful schemes have been orbiting transition state/phase space theory (OTS/PST) such as elaborated by Chesnavich and Bowers (see *e.g.* [2–5]), phase space theory involving the concept of product temperatures (PST, T^*) by Klots (see *e.g.* [6–8]), variational flexible transition state RRKM theory with exit channel coupling (VRRKM/ECC) by Wardlaw, Marcus, Klippenstein, *et al.* (see *e.g.* [9–11]), the separate statistical ensembles (SSE) model by Wittig *et al.* [12], and the statistical adiabatic channel model (SACM) [13]. Comparison with experimental TPEDs often showed good agreement with OTS/PST calculations. Dissociations with large barriers in the reverse direction gave rise to enhanced kinetic energy release (KER).

The success of OTS/PST may appear troubling for the following reasons. While TPEDs appear to be modeled adequately by loose activated complex PST, specific rate constants $k(E)$ of ion fragmentation traditionally are represented by rigid activated complex RRKM theory with oscillator-type transition states. $k(E)$ as well as the corresponding thermally averaged high pressure dissociation rate constants $k_\infty(T)$ are often far below OTS/PST calculations. Thus, there seems to be an inconsistency which deserves further investigation. The present article addresses this subject for the fragmentation of *n*-propylbenzene cations as a representative example of a simple bond fission without reverse barrier. The reaction predominantly proceeds via a C–C bond fragmentation,

$$n\text{-}C_9H_{12}{}^+ \rightarrow C_7H_7{}^+ + C_2H_5\,. \tag{1.1}$$

Specific rate constants $k(E)$ for this reaction have been measured by Kim *et al.* using laser photodissociation and MIKES [14] and we have recently measured thermal dissociation rate constants [15]. $k(E)$ was analysed in [14] by rigid activated complex RRKM theory, whereas TPEDs were represented by OTS/PST. In contrast to this, we modeled $k(E, J)$ by SACM/CT (statistical adiabatic channel model/classical trajectories) calculations [15, 16]. While it appears difficult to combine RRKM and OTS/PST into one internally consistent scheme, this is not the case with SACM/CT. This approach allows one to generate $k(E, J)$ and TPEDs as a function of energy E and angular momentum (quantum number J) in a consistent manner. The present work describing SACM/CT calculations of TPEDs for reaction (1.1) complements [15] and [16] where $k(E, J)$ and $k_\infty(T)$ were modeled using the same potential.

2. Calculational method

2.1 SACM/CT concept

Since the concept of the statistical adiabatic channel model often is misrepresented (even in the monograph [1]), the principles of our approach are briefly summarized in the following: (i) The internal modes of the reactant and the fragments are compared in order to identify conserved and transitional (disappearing) modes. The conserved modes, to a first approximation, are identified with the internal modes of the fragments. In dissociation, the conserved modes are assumed to stay adiabatically in their respective quantum states during the final separation of the fragments (or during the initial approach of the fragments in the reverse association). In other words, our approach assumes vibrational adiabaticity in the conserved modes. (ii) The dynamics of the dissociation is divided into two stages. During the first stage, intramolecular vibrational redistribution (IVR) or other processes (such as collisions) are assumed to establish a statistical distribution of reactant states. During the second stage, the fragments must pass dynamical bottle-necks created by the anisotropy of the potential and/or by centrifugal effects before separation occurs. Not all trajectories are successful at passing the bottle-neck. The reverse association starts from a statistical distribution of reactants and the combining fragments must pass the same dynamical bottle-necks for association to occur. In the second stage then capture is terminated by IVR or by collisions. The assumptions of vibrational adiabaticity and of statistical distributions at the beginning of the final separation of the dissociation fragments provide a considerable simplification of the treatment of the complete dynamics. However, these assumptions are not necessarily valid and need to be justified. (iii) The dynamics of the transitional modes during the second stage of dissociation (or the reverse first stage of association) is treated explicitly on a potential energy surface (PES) of reduced dimensionality, *i.e.* on a PES with frozen conserved modes. The dynamics of transitional modes may be rotationally adiabatic or nonadiabatic, in the limit being "sudden", see below. The extent of the nonadiabaticity is governed by the effective mass M of the system or the corresponding Massey parameter $\xi = \sqrt{2M}$ which corresponds to the ratio of the effective rotational period of the transitional modes and the collision time on the reduced dimensionality PES. In the adiabatic limit (*i.e.*, in the limit $\xi \gg 1$), the motion proceeds on one-dimensional adiabatic channel potential curves which can be constructed by determining the eigenvalues of the transitional modes at frozen interfragment center-of-mass distances. In the earliest version of SACM [17], these eigenvalues were approximated by exponential interpolations between reactant and fragment eigenvalues assuming a non-crossing rule. In later versions of SACM (see *e.g.* [18–23]), eigenvalues were calculated accurately for simple model potentials. There are avoided crossings of the adiabatic channel potentials, few for atom + linear capture and numerous for linear + linear capture. Nonadiabatic transitions occur at such crossings or over broader ranges of

distances, Coriolis coupling being of particular importance [24]. Nonadiabatic dynamics (in the limit being "sudden", *i.e.*, $\xi \ll 1$) most conveniently is treated by classical trajectory (CT) calculations. It was shown [25] that adiabatic channel and CT treatments in the range of classical and adiabatic dynamics lead to identical results. Therefore, SACM/CT appears to be the method of choice. Refined versions of variational transition state theory that include dynamical corrections [26] and the SACM/CT outlined here appear to yield similar results if they are applied to the same PES. However, in both cases CT calculations are essential for an accurate characterization of the transitional mode dynamics.

Specific rate constants $k(E, J)$ within the SACM/CT concept are represented by the well-known relationship from statistical unimolecular theory [1]

$$k(E, J) = W(E, J)/h\rho(E, J) \tag{2.1}$$

where $\rho(E, J)$ denotes the rovibrational density of states of the reactant molecule. The contribution of the transitional modes to $W(E, J)$ in SACM/CT is given by the number of quantum states $W_0(E, J)$ of the separated fragments at a given E and J multiplied with the capture probability $w(E, J)$ such as derived by CT calculations. In the limit of adiabatic dynamics, this product corresponds to the number of adiabatic channels which are open in association or in the reverse dissociation. In the case of nonadiabatic dynamics, axially nonadiabatic versions of SACM [24] or CT [25] calculations are used for the determination. Compared to a variational treatment applied to phase space volumes such as used in VTST, the SACM/CT approach has the advantage of automatically including dynamical corrections. The total $W(E, J)$ finally is obtained by convolution of the contribution from the transitional modes with the contribution from the quantized conserved modes such as this is usual in statistical unimolecular rate theory [1].

For the present purpose, Eq. (2.1) is further specified by selecting trajectories in CT capture calculations with a given property of interest, *e.g.* a specific product translational or rotational energy. Collecting those initial states from the phase space of the separated fragments, *e.g.*, with given translational energies E_{tr} which lead to capture, gives $W(E, J, E_{tr})$. The derived TPEDs then are given either in cumulative, integral, form as

$$P(E, J, E_{tr}) = \int_0^{E_{tr}} W\left(E, J, E'_{tr}\right) \mathrm{d}E'_{tr} \Big/ \int_0^{E} W\left(E, J, E'_{tr}\right) \mathrm{d}E'_{tr} \tag{2.2}$$

or in differential form by $\mathrm{d}P(E, J, E_{tr})/\mathrm{d}E_{tr}$. For calculational purposes and representational reasons in the present work we prefer the integral form of Eq. (2.2) over the differential form. Vibrational and rotational energy distributions can be determined in an analogous manner. For details of our CT calculations, see [25].

The described SACM/CT calculation of TPEDs is consistent with the SACM/CT determination of $k(E, J)$ and of $k_\infty(T)$. Our concept of determining TPEDs from CT capture calculations is not completely new. It corresponds to the rudimentary treatment for a simple triatomic system by Hamilton and Brumer [27]. It should finally be emphasized that in applying CT calculations to the transitional mode dynamics, zeropoint energy problems are negligible for most conditions of interest. However, at ultralow temperatures or energies very close to threshold, the corresponding quantum effects could also be accounted for in the usual way by SACM or by axially nonadiabatic SACM such as discussed in [24].

2.2 Potential energy surface

The described SACM/CT concept can be applied to *ab initio* PESs, whenever these are available [28], or to modeled PESs. For the CT part of the treatment, reduced dimensionality PESs of the transitional modes are required. *Ab initio* PESs generally are not yet available or accurate enough in the range of interfragment center-of-mass distances r where the dynamical bottle-necks are located (see *e.g.* the N_4^+ potential considered in [29] and [30]). Therefore, one often has to live with modeled, hopefully realistic, PESs. In the present case, we had to construct a model potential which reproduces the essential features of $C_9H_{12}^+$ and of the fragments $C_7H_7^+ + C_2H_5$ and which characterizes their interaction in a simplified manner. This required at least one fit parameter which was adjusted by comparison with experimental $k(E)$. After that, no further adjustments were made. Our PES was described in detail in [16] and is only briefly summarized in the following.

We separate the PES of the transitional modes into the sum of a radial and an angular part, $V(r)$ and $V(r, \text{angles})$ respectively. The radial part is characterized by a switching between a short-range valence potential $V^{\mathrm{SR}}(r)$ of Morse type and a long-range modified electrostatic (in the present case ion-induced dipole) potential $V^{\mathrm{LM}}(r)$ where

$$V^{\mathrm{SR}}(r) = E_0\{\exp[-2\beta(r-r_\mathrm{e})] - 2\exp[-\beta(r-r_\mathrm{e})]\} \tag{2.3}$$

and

$$V^{\mathrm{LR}}(r) \approx -\frac{\alpha q^2/2}{(r-\Delta r_\mathrm{B})^4 + \alpha q^2/2D} \tag{2.4}$$

with $\Delta r_\mathrm{B} = r_\mathrm{e} - r_\mathrm{Be}$. r_Be represents the equilibrium value of the length of the forming or breaking bond and r_e is the equilibrium value of the c.o.m.-distance between the fragments. At large r, *i.e.* $r \gg \Delta r_\mathrm{B}$ and $r^4 \gg \alpha q^2/2D$, $V^{\mathrm{LR}}(r)$ approaches the ion-induced dipole potential $-\alpha q^2/2r^4$. The switching between $V^{\mathrm{SR}}(r)$ and $V^{\mathrm{LR}}(r)$ is performed by the expression

$$V(r) = V^{\mathrm{SR}}(r)[1-\kappa F] + V^{\mathrm{LR}}(r)F \tag{2.5}$$

with

$$F = 1/\{1 + \exp[-2\beta(r - r_{sw})]\} \tag{2.6}$$

and

$$\kappa = 1 - \frac{\alpha q^2}{E_0(r_{sw} - \Delta r_B)^4} \,. \tag{2.7}$$

r_{sw} denotes that value of r where $V^{SR}(r)$ and $V^{LR}(r)$ from Eqs. (2.3) and (2.4) intersect. The relevant parameters for reaction (1.1) were chosen as $E_0/hc = 13\,950\,\mathrm{cm}^{-1}$, $\beta = 5.13\,\text{Å}^{-1}$, $r_e = 4.74\,\text{Å}$, $\alpha(C_2H_5) = 4.27\,\text{Å}^3$, $r_{Be} = 2.42\,\text{Å}$, $r_{sw} = 5.14\,\text{Å}$, see [16].

The angular potential is represented by an anisotropy of dipole–dipole type, with an amplitude which exponentially decreases with increasing r, through

$$V(r, \text{angles}) = C \exp[-\beta(r - r_e)]\left\{\left[2 + \boldsymbol{d}_1\boldsymbol{d}_2 - 3(\boldsymbol{d}_1\boldsymbol{n})(\boldsymbol{d}_2\boldsymbol{n})\right]/4\right\} . \tag{2.8}$$

$\boldsymbol{d}_1$ and $\boldsymbol{d}_2$ are unit vectors along the axes of the fragments, $\boldsymbol{n}$ is the unit vector along the line connecting the c.o.m.s. The amplitude of the anisotropy in principle corresponds to that of the valence potential. In practice, however, we treat this as a fit parameter to reproduce measured values of $k(E)$. In the present case, for illustrative purposes, $C/E_0 \approx 20$ was chosen like in [16]. The value of C is of particular importance since it defines the deviation from PST which is characterized by $C = 0$; the particular shape of the angular dependence in Eq. (2.8) is only of much smaller relevance. *E.g.*, in [16] we also studied anisotropies of ion–permanent dipole type which led to similar results, however, with a different anisotropy amplitude factor.

In order to simplify our CT calculations in the extensive calculations described below, both $C_7H_7^+$ and C_2H_5 were treated as linear rotors with the effective rotational constants $B_1/hc = (0.18 \times 0.094 \times 0.062)^{1/3}\,\mathrm{cm}^{-1} = 0.102\,\mathrm{cm}^{-1}$ and $B_2/hc = (3.51 \times 0.753 \times 0.699)^{1/3}\,\mathrm{cm}^{-1} = 1.23\,\mathrm{cm}^{-1}$ respectively. In order to classify the capture dynamics of the transitional modes with respect to the degree of rotational adiabaticity, we consider an average Massey parameter which is given by [16]

$$\xi \approx (2\mu B)^{1/2}/\hbar\beta \tag{2.9}$$

with $B \approx (B_1 + B_2)/2$. This Massey parameter is equal to $\xi \approx 0.18$. Thus, the dynamics of the transitional rotational modes is not adiabatic but on the way to sudden dynamics ($\xi \ll 1$). On the other hand, the dynamics of the conserved vibrational modes is adiabatic ($\xi \gg 1$). This is found by replacing B in Eq. (2.9) by vibrational quanta.

3. CT calculations of product energy distributions

3.1 Centrifugal barriers

Translational product energy distributions are markedly influenced by angular momentum conservation constraints as well as by the centrifugal barriers $E_0(J)$ arising from the PES. In the simplest version of phase space theory, $E_0(J)$ would simply be put equal to zero. Larger kinetic energy release is obtained in OTS/PST where $E_0(J)$ is derived from the electrostatic long-range potential. In SACM/CT we go one step further by determining $E_0(J)$ from the complete PES except that the anisotropy is artificially switched off. A radial potential is employed which accounts for the complete short-range valence/long-range electrostatic potential. This contrasts to the artificial limitation of only a long-range potential used in OTS/PST. In other words, we calculate $E_0(J)$ from the complete minimum energy path of the PES.

$E_0(J)$ was either obtained by CT calculations or by determining the maxima of the effective potentials $V(r) + L(L+1)\hbar^2/2\mu r^2$ with $V(r)$ from Eq. (2.5) (L = orbital angular momentum quantum number); the approximation $J \approx L$ in the present case can be used for most conditions, see [16]. The results from both methods can be represented by

$$E_0(J)/hc \approx 5.90 \times 10^{-7}\ \mathrm{cm}^{-1}\left\{[J(J+1)]^2/\left[1 + 9.73 \times 10^{-3} J^{1.075} + 5.21 \times 10^{-6} J^{2.166}\right]\right\}. \tag{3.1}$$

Eq. (3.1) illustrates the differences between our PST and OTS/PST for which $E_0(J)$ would be given by

$$E_0(J) = \left[J(J+1)\hbar^2/2\mu\right]^2/2\alpha q^2, \tag{3.2}$$

i.e. from Eq. (3.1) with the denominator put equal to unity. One notices that the short-range valence part of the potential at large J reduces $E_0(J)$ in comparison to that found from only the long-range potential. As a consequence at high temperatures, the present $k_\infty^{\mathrm{PST}}(T)$ slightly exceeds the Langevin capture rate constant, $k_\mathrm{L} = 2\pi q(\alpha/\mu)^{1/2}$, which would be the result from OTS/PST, see [16].

3.2 Specific capture probalitities *w(E, J)* and rigidity factors $f_{\mathrm{rig}}(E, J)$

Product energy distributions are most conveniently interpreted by looking first at overall capture probabilities, $w(E, J)$, for which the product energies are not yet specified. For this reason, in Fig. 1a–c we present capture probabilities $w(E, J)$ and PST capture probabilities $w^{\mathrm{PST}}(E, J)$ for $J = 0$, 100, and 200, respectively. In Fig. 2a–c specific rigidity factors,

$$f_{\mathrm{rig}} = w(E, J)/w^{\mathrm{PST}}(E, J), \tag{3.3}$$

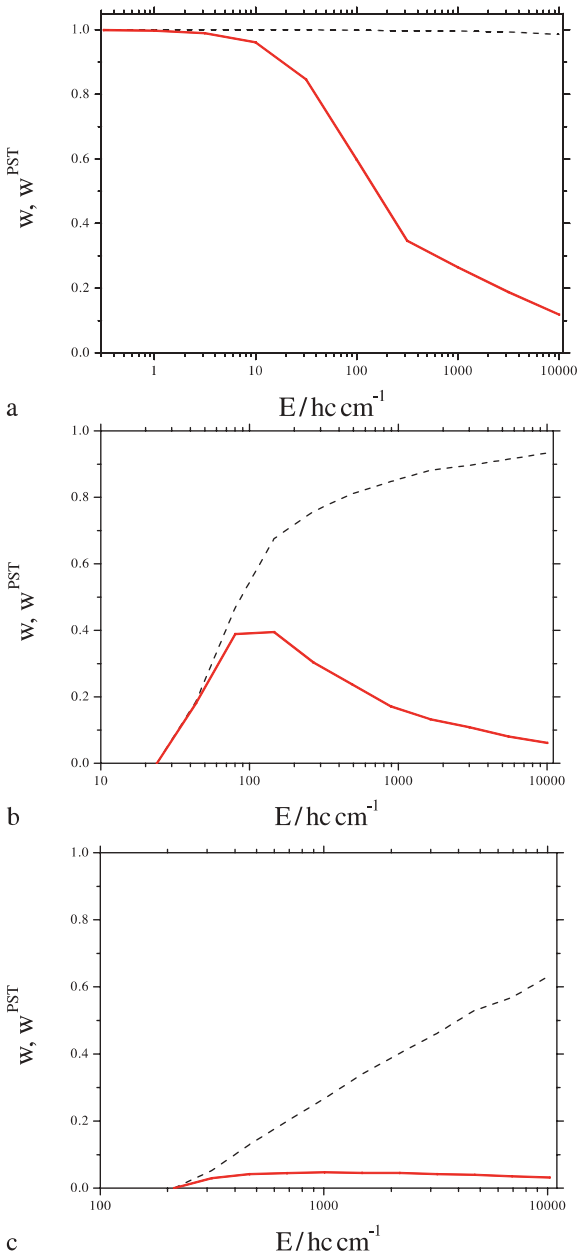

Fig. 1. Capture probabilities $w(E, J)$ (full lines) and capture probabilities $w^{\mathrm{PST}}(E, J)$ from phase space theory (dashed lines) for the dissociation of *n*-propylbenzene cations. SACM/CT calculations from this work for $J = 0$ (Fig. 1a, $E_0(J) = 0$), $J = 100$ (Fig. 1b, $E_0(J)/hc = 23.8\,\mathrm{cm}^{-1}$), and $J = 200$ (Fig. 1c, $E_0(J)/hc = 214\,\mathrm{cm}^{-1}$).

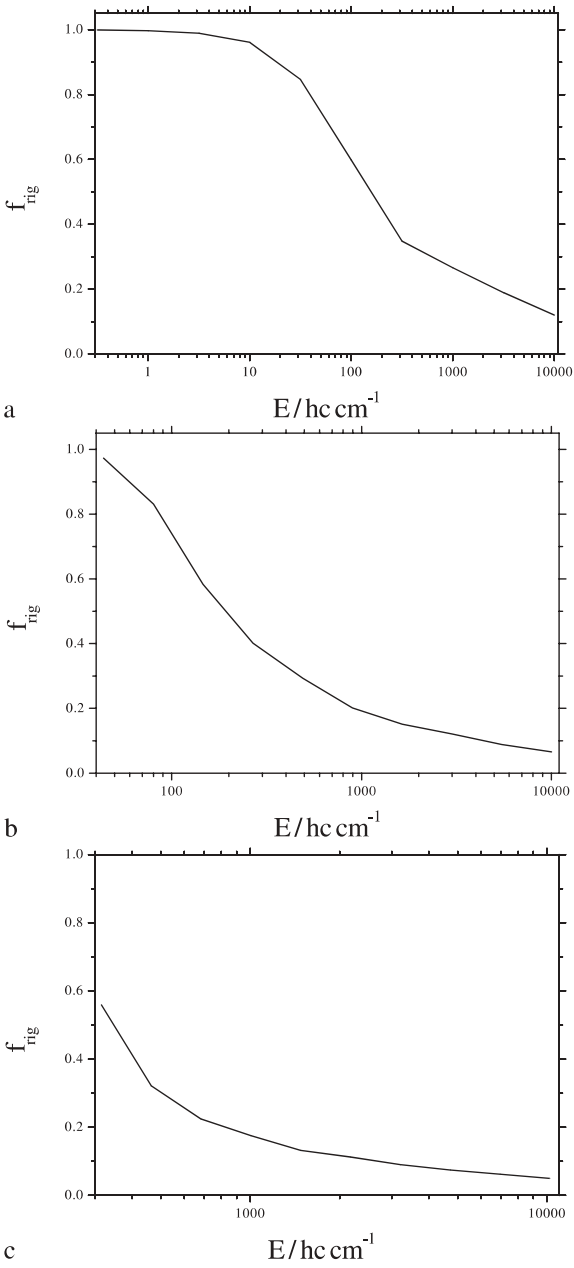

Fig. 2. Specific rigidity factors $f_{\text{rig}} = w(E, J)/w^{\text{PST}}(E, J)$, with the results from Fig. 1, for $J = 0$ (Fig. 2a), $J = 100$ (Fig. 2b), and $J = 200$ (Fig. 2c).

are plotted as a function of the energy E and at the same fixed angular momenta ($J = 0$, 100, and 200). PST where centrifugal barriers are neglected would give $w^{\mathrm{PST}}(E, J) = 1$, such that $W(E, J) = W_0(E, J)$ would correspond to the well-known statistical expressions given in [5, 31–33] (before convolution with the conserved modes). $w^{\mathrm{PST}}(E, J)$ in the present case can well be approximated by

$$w^{\mathrm{PST}}(E, J) \approx (1 - E_0(J)/E)^2 \tag{3.4}$$

which corresponds to the large J-approximation ($J \approx L$). According to the differences in $E_0(J)$ such as quantified by Eq. (3.1), OTS/PST and our present PST through Eq. (3.4) have slightly different values of $w^{\mathrm{PST}}(E, J)$. Fig. 1a–c illustrate the effects of $E_0(J)$ on $w^{\mathrm{PST}}(E, J)$. The decrease of $w(E, J)$ from $w^{\mathrm{PST}}(E, J)$ arises from the anisotropy of the potential such as illustrated in Fig. 1a–c. The observed effects are easily interpreted. At low energies not far above $E_0(J)$, the dynamical bottle-necks are located at large c.o.m. distances where the PES is not very anisotropic. With increasing energies and increasing J, these bottle-necks move to smaller values of r where the increasing anisotropy enhances the constraints and $w(E, J)$ increasingly falls below $w^{\mathrm{PST}}(E, J)$. This effect is seen particularly clearly in Fig. 2a–c. One may expect that the corresponding "rigidity effects" also become apparent in the TPEDs described in the following.

3.3 Translational product energy distributions

Fig. 3a–c compare cumulative TPEDs defined by Eq. (2.2) for the anisotropic model PES of reaction (1.1) with the corresponding TPEDs for the artificially isotropic model PES characterizing our PST. Our CT results, for fixed J, are plotted as a function of the product translational energy divided by the total energy E_{total}. It should be noted that, in our work, the zeropoint of the energy scale is put at the lowest possible rovibrational energy of the separated fragments. In order to emphasize the translational, rotational, and vibrational contributions to the energy, the energy E is also called E_{total}. Near to $E = 0$ where vibrations cannot be excited, $E = E_{\mathrm{total}} = E_{\mathrm{tr}} + E_{\mathrm{rot}}$ such that $P(E, J, E_{\mathrm{rot}}) = 1 - P(E, J, E_{\mathrm{tr}})$. For larger E_{vib}, the relation is more complicated but can be reconstructed from Figs. 3–5. Vibrations are always treated quantized while rotations and translations are classical.

A number of observations are worth mentioning: (i) For small values of E_{total}, the TPEDs do not differ too much from the distributions from PST. However, with increasing E_{total}, the TPEDs are increasingly moving to the left, *i.e.* there is increasingly more KER than in PST. (ii) For $J = 0$, the cumulative TPEDs can be representated well by $1 - \exp(-E_{\mathrm{tr}}/\langle E_{\mathrm{tr}}\rangle)$. This corresponds to exponential differential TPEDs, $\exp(-E_{\mathrm{tr}}/\langle E_{\mathrm{tr}}\rangle)$. With increasing J and small E_{total}, however, this changes into differential TPEDs of the type $E_{\mathrm{tr}}^n \exp(-E_{\mathrm{tr}}/\langle E_{\mathrm{tr}}\rangle)$. (iii) With increasing E_{total}, the average KER $\langle E_{\mathrm{tr}}\rangle$ rises increasingly above $\langle E_{\mathrm{tr}}\rangle$ from PST. Our PST results correspond to the typical

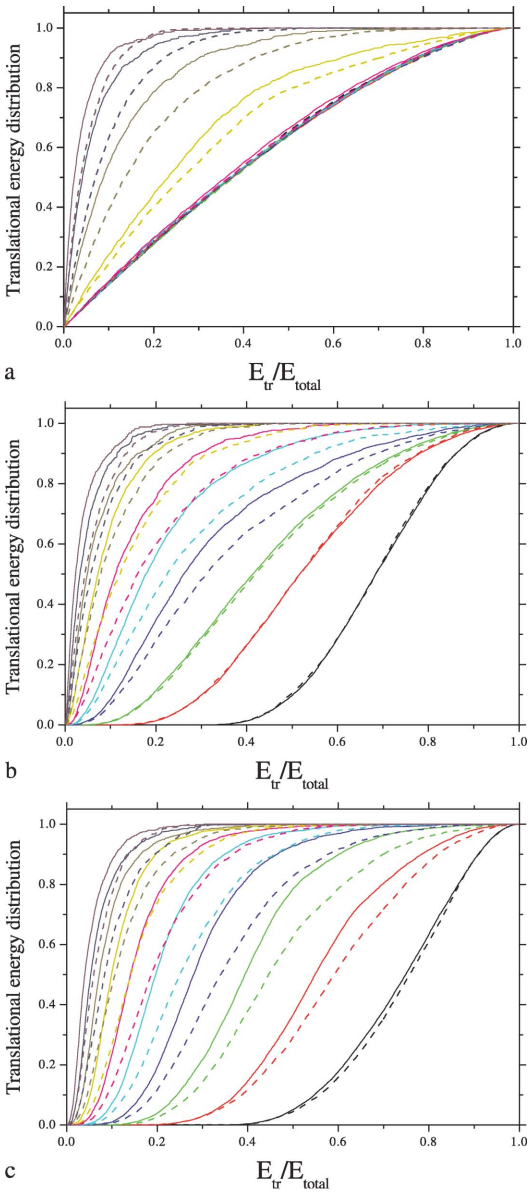

Fig. 3. Cumulative translational product energy distributions (Eq. (2.2)) in the dissociation of *n*-propylbenzene cations. SACM/CT calculations from this work for the full anisotropic potential (full lines) and for the artificially isotropic potential (PST, dashed lined). Curves from left to right: E_{total}/hc cm^{-1} = 10 000, 3160, 1000, 316, 100, 31.6, 10, 3.16, 1, and 0.316 for $J = 0$ (Fig. 3a), E_{total}/hc cm^{-1} = 10 024, 5480, 2996, 1638, 896, 490, 268, 146, 80, 43.7 for $J = 100$ (Fig. 3b), and E_{total}/hc cm^{-1} = 10 214, 6939, 3203, 2176, 1479, 1005, 682, 464, 315 for $J = 200$ (Fig. 3c).

behaviour of PST such as described, *e.g.* in [1–8]. The deviations from the TPEDs of PST are caused by the anisotropy of the PES.

We do not intend at this stage to provide further quantitative analysis of the TPEDs of Fig. 3a–c. However, we note that increasing deviations of TPEDs from OTS/PST with increasing energy have also been observed experimentally, *e.g.* in the dissociation $CH_3I^+ \rightarrow CH_3^+ + I$ [35, 36]. Exponential differential TPEDs have also been observed experimentally [35–38]. However, our calculations show that one must expect deviations from this behaviour with increasing J and, in particular, if the fragments both are not monatomic. It has been suggested that $\langle E_{tr} \rangle$ should be proportional to E_{total} [39] (see the representation of results for $CH_3COCH_3^+ \rightarrow CH_3CO^+ + CH_3$ in [40]). Fig. 3a shows that there is a range at small E_{total} (and small J) where such a behaviour is also observed in our calculations. However, with increasing E_{total} both in PST and in the general PES the ratio $\langle E_{tr} \rangle / E_{total}$ obviously decreases, finally reaching a stationary value of $\langle E_{tr} \rangle$ independent of E_{total}.

3.4 Rotational and vibrational product energy distributions

Our CT calculations also allowed for the specification of product rotational and vibrational energy distributions. We illustrate the corresponding cumulative distributions in Figs. 4 and 5, again as a function of the energies relative to E_{total} and as a function of angular momentum. The quantum nature of the distributions after convolution with the conserved modes becomes quite apparent, particularly in the vibrational energy distributions, see Fig. 5a–c, but also in the rotational distributions of Fig. 4a–c where the most pronounced "irregularities" arise at an energy where the first vibrational levels of the fragments can be excited.

We do not intend to further analyze the fine details of the distributions here but we emphasize that there are ranges where the distributions markedly differ from the PST distributions. The differences are not so much in the shape of the distribution functions but more in the average energies $\langle E_{rot} \rangle / E_{total}$ and $\langle E_{vib} \rangle / E_{total}$. The specific properties of the vibrational and rotational energy distributions depend on the specific molecular parameters of the considered reaction systems. Not all details of Figs. 3–5, therefore, may be expected to be found in other reaction systems.

4. Conclusions

The present SACM/CT calculations of product energy distributions in the fragmentation of *n*-propylbenzene cations have shown that PST provides more or less realistic shapes of the distribution functions. However, the average translational, rotational, or vibrational energies of the fragments are close to the values from PST only for small J and small energies E. At larger E and J, one

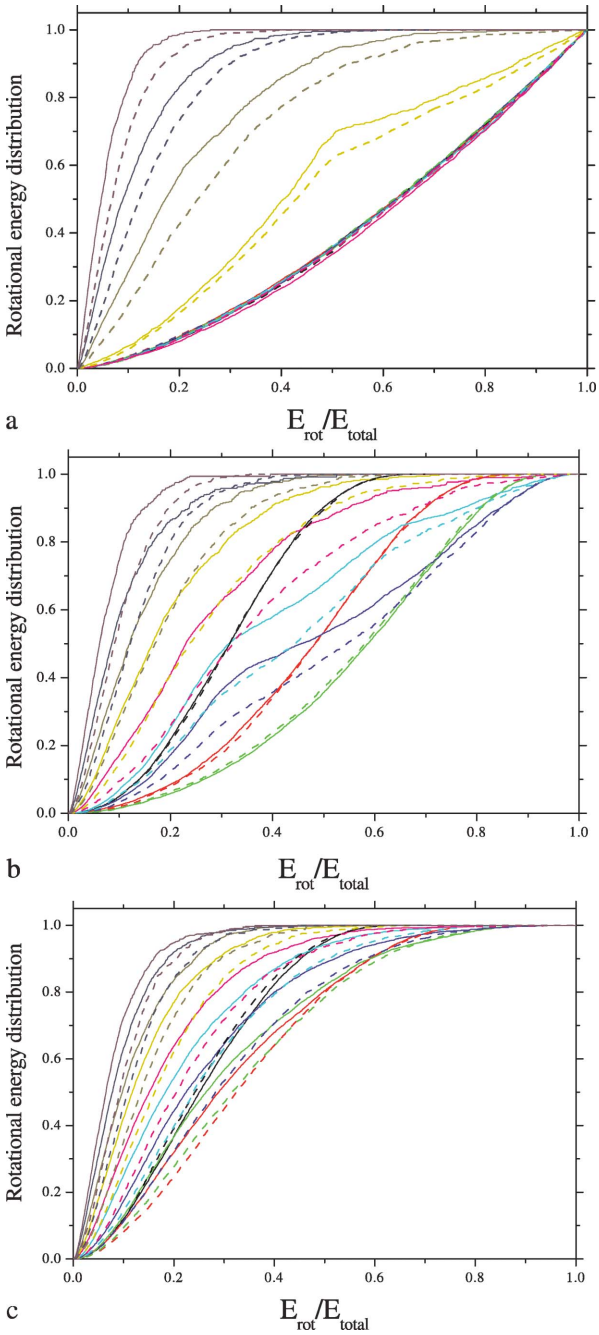

Fig. 4. As Fig. 3 for rotational product energy distributions.

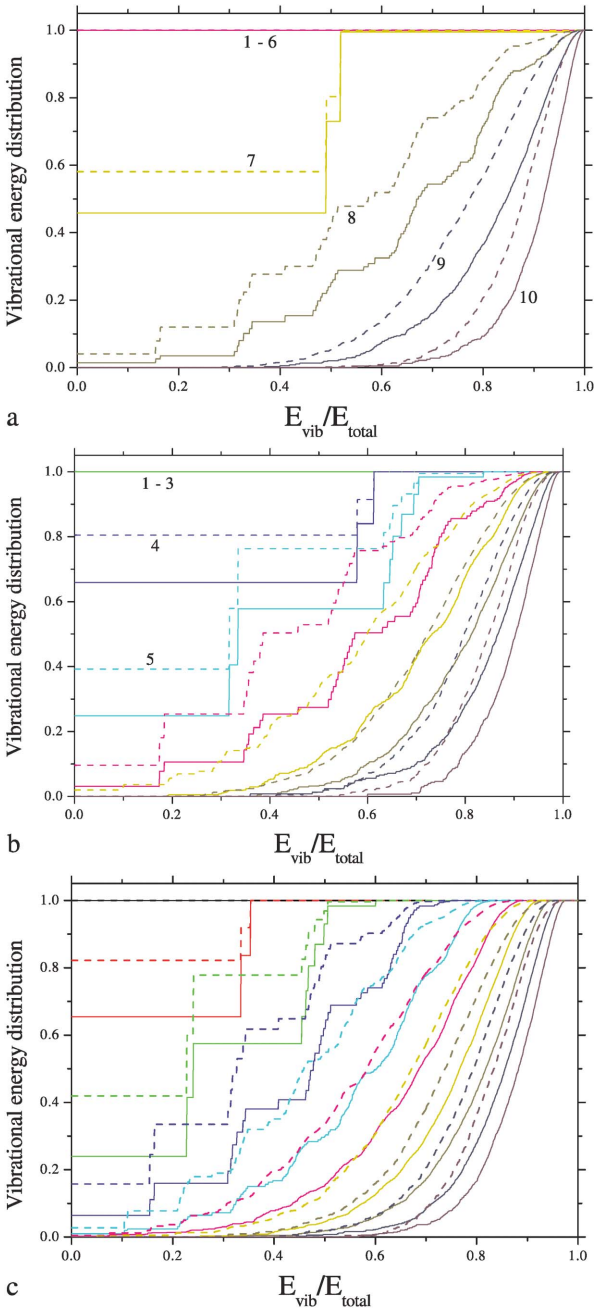

Fig. 5. As Fig. 3 for vibrational product energy distributions, however, with curves from right to left for the indicated values of E_{total}.

has to expect increasing differences from PST. This behaviour is due to the shift of the effective bottle-necks of the reaction from the isotropic long range (ion-induced dipole) part of the potential into the increasingly anisotropic region of the short-range valence potential. The corresponding behaviour has also been observed in our previous SACM/CT modellings of the specific rate constants $k(E, J)$ and the thermally averaged dissociation rate constants $k_\infty(T)$ of the reaction. More studies of product energy distributions by the present type of SACM/CT capture calculations for other dissociation processes appear desirable.

Acknowledgement

Many inspiring discussions with Professor Jürgen Wolfrum are gratefully acknowledged. This work has been supported by funding through the Deutsche Forschungsgemeinschaft (SFB 357 "Molekulare Mechanismen unimolekularer Prozesse"), the European Office for Aerospace Research (EOARD Grant No. FA 8655-03-1-3034) and the United States Air Force Office of Scientific Research (Project 2303 EP4).

References

1. T. Baer and W. L. Hase, *Unimolecular Reaction Dynamics. Theory and Experiment*, Oxford University Press, New York, Oxford (1996).
2. W. J. Chesnavich and M. T. Bowers, J. Am. Chem. Soc. **98** (1976) 8301.
3. W. J. Chesnavich and M. T. Bowers, J. Chem. Phys. **66** (1977) 2306.
4. W. J. Chesnavich and M. T. Bowers, J. Am. Chem. Soc. **99** (1977) 1705.
5. W. J. Chesnavich and M. T. Bowers, in *Gas Phase Ion Chemistry, Vol. 1*, M T. Bowers (Ed.), Academic Press, New York, San Francisco, London (1979), p. 119.
6. C. E. Klots, J. Chem. Phys. **98** (1993) 206; **100** (1994) 1035.
7. C. E. Klots, J. Phys. Chem. **99** (1995) 1748.
8. C. E. Klots, in *Unimolecular and Bimolecular Ion Molecule Reaction Dynamics*, T. Baer, C. Y. Ng, and I. Powis (Eds.), Wiley, New York (1994), p. 311.
9. D. M. Wardlaw and R. A. Marcus, Adv. Chem. Phys. **70** (1988) 231.
10. S. J. Klippenstein, L. R. Khundkar, A. H. Zewail, and R. A. Marcus, J. Chem. Phys. **89** (1988) 4761.
11. S. J. Klippenstein and R. A. Marcus, J. Chem. Phys. **91** (1989) 2280.
12. C. Wittig, I. Nadler, H. Reisler, M. Noble, J. Catanzarite, and G. Radhakrishnan, J. Chem. Phys. **83** (1985) 5581.
13. M. Quack and J. Troe, Ber. Bunsenges. Phys. Chem. **79** (1975); L. Brouwer, C. J. Cobos, J. Troe, H.-R. Dübal, and F. F. Crim, J. Chem. Phys. **86** (1987) 6171.
14. W. G. Hwang, J. H. Moon, J. C. Choe, and M. S. Kim, J. Phys. Chem. A **102** (1998) 7512.
15. A. I. Fernandez, A. A. Viggiano, Th. M. Miller, S. Williams, I. Dotan, J. V. Seeley, and J. Troe, J. Phys. Chem. A **198** (2004) 9652.
16. J. Troe, V. G. Ushakov, and A. A. Viggiano, Z. Phys. Chem. **219** (2005) 715.
17. M. Quack and J. Troe, Ber. Bunsenges. Phys. Chem. **78** (1974) 240.
18. J. Troe, J. Chem. Phys. **87** (1987) 2773; **105** (1996) 6249.

19. S. Smith and J. Troe, J. Chem. Phys. **97** (1992) 5451.
20. A. I. Maergoiz, E. E. Nikitin, and J. Troe, J. Chem. Phys. **95** (1991) 5117; Z. Phys. Chem. **172** (1991) 129.
21. K. Takayanagi, J. Phys. Soc. Jpn. **45** (1978) 976; K. Sakimoto, Chem. Phys. **68** (1982) 155; **85** (1984) 273.
22. N. Markovic and S. Nordholm, J. Chem. Phys. **91** (1989) 6813; N. Markovic, Chem. Phys. **188** (1994) 73.
23. M. L. Dubernet and R. Mc Carroll, Z. Phys. D **13** (1989) 255; **15** (1990) 333.
24. E. I. Dashevskaya, I. Litvin, E. E. Nikitin, and J. Troe, J. Chem. Phys. **120** (2004) 9989.
25. A. I. Maergoiz, E. E. Nikitin, J. Troe, and V. G. Ushakov, J. Chem. Phys. **105** (1996) 6263, 6270, 6277; **108** (1998) 5265, 9987.
26. S. J. Klippenstein, Y. Georgievskii, and L. B. Harding, Proc. Combust. Inst. **29** (2002) 1229.
27. I. Hamilton and P. Brumer, J. Chem. Phys. **82** (1985) 595.
28. L. B. Harding, J. Troe, and V. G. Ushakov, Phys. Chem. Chem. Phys. **2** (2000) 631.
29. C. Léonard, P. Rosmus, S. Carter, and N. C. Handy, J. Phys. Chem. A **103** (1999) 1846.
30. J. Troe, Phys. Chem. Chem. Phys. **7** (2005), in press.
31. J. Troe, J. Chem. Phys. **79** (1983) 6017.
32. M. Olzmann and J. Troe, Ber. Bunsenges. Phys. Chem. **96** (1992) 1327; **98** (1994) 1563.
33. C. E. Klots and J. Polách, J. Phys. Chem. **99** (1995) 15396.
34. A. I. Maergoiz, E. E. Nikitin, J. Troe, and V. G. Ushakov, J. Chem. Phys. **117** (2002) 4201.
35. D. M. Mintz and T. Baer, J. Chem. Phys. **65** (1976) 2407; T. Baer, Adv. Chem. Phys. **64** (1986) 111.
36. I. Powis, Chem. Phys. **74** (1983) 421.
37. K. Johnson, I. Powis, and C. J. Danby, Chem. Phys. **63** (1981) 1.
38. I. Powis, Acc. Chem. Res. **20** (1987) 179.
39. M. A. Haney and J. L. Franklin, J. Chem. Phys. **48** (1968) 4093.
40. T. Baer, in *Gas Phase Ion Chemistry, Vol. 1*, M. T. Bowers (Ed.), Academic Press, New York, San Francisco, London (1979), p. 153.